

## CHAPTER IV

### RESULT AND DISCUSSION



#### 4.1 Preparation and Characterization of Chitosan

##### 4.1.1 Chitosan Production

Shrimp shells consist of three major components which are chitin, calcium carbonate, and protein. Calcium carbonate and protein can be removed by solvent extraction and chitin will be obtained as the remaining substance. Where as chitosan is the name given to the total, partially (majorly) deacetylated form of chitin.

In this research, chitosan was prepared from shells of *Penaeus merguensis* shrimp by demineralization with HCl, deproteinization with 4% NaOH and deacetylation with 50% NaOH in order to remove the calcium carbonate, protein, and the acetyl group of N-acetyl glucosamine repeating units in shrimp shells, respectively.

**Table 4.1** Yield of chitin and chitosan production from shrimp shell

Materials	Yield*(%)
Shrimp shell	100
Product after demineralization	49.65
Product after deproteinization (chitin)	30.63
Product after deacetylation (chitosan)	23.35

\* dry weight basis

##### 4.1.2 Determination of the Degree of Deacetylation (%DD) of Chitosan

The method used to determine degree of deacetylation of chitosan was based on infrared spectroscopic measurement by Sannan *et al.* (1978). The degree of deacetylation (%DD) was calculated from equation 4.1.

$$DD(\%) = 98.03 - 34.68(A_{1550}/A_{2878}) \quad (4.1)$$

where  $A_{1550}$  and  $A_{2878}$  are absorbance at  $1550 \text{ cm}^{-1}$  and  $2878 \text{ cm}^{-1}$ , respectively.

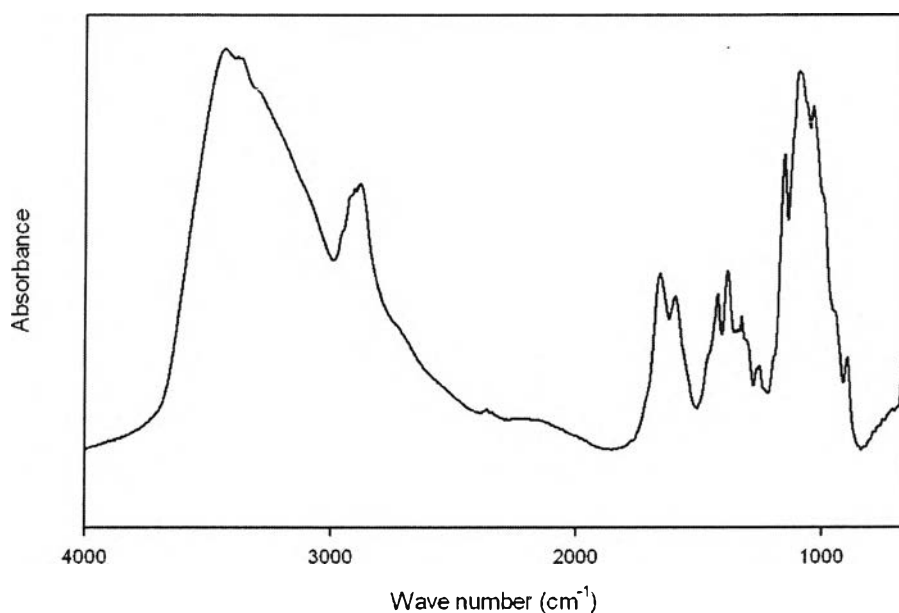


**Figure 4.1** FTIR spectrum of chitosan powder.

Chitosan has more extent of amino groups than acetamide groups at C2 position of N-acetyl glucosamine repeating units. The degree of deacetylation of chitosan depends on the nature of chitosan resources and the conditions used during deproteinization. The chitosan used in this study was inevitably subjected to N-deacetylation process under alkaline condition and heating. According to the method of Sannan *et al.* (1978), the degree of deacetylation of chitosan calculated from FTIR spectrum was 80%.

#### 4.1.3 Determination of the Molecular Weight of Chitosan

The molecular weight of chitosan was determined based on viscosity measurement by the method of Wang *et al.* (1991). The viscosity-average molecular weight of chitosan was calculated via Mark-Houwink equation (equation 4.2)

$$[\eta] = 6.59 \times 10^{-5} M_v^{0.88} \quad (4.2)$$

where  $[\eta]$  = Intrinsic viscosity (dl/g)  
 $M_v$  = Viscosity-average molecular weight

The intrinsic viscosity was determined from the Y-intercept of the plot between  $[\eta_{sp}]/c$  versus chitosan concentration (g/dl) and  $\ln [\eta_{rel}]/c$  versus chitosan concentration (g/dl). The intrinsic viscosity was obtained at 12.161 dl/g. the viscosity-average molecular weight of chitosan was  $9.67 \times 10^5$  g/mole.

#### 4.1.4 X-Ray Diffractometry (XRD)

The x-ray diffraction patterns of chitosan powder and chitosan film are illustrated in Figure 4.2. The diffraction peak at approximately  $2\theta = 11^\circ$  and  $20^\circ$  was observed in the diffraction pattern of chitosan powder indicating the crystalline state of the powder. After being solution casting, the broad peak centered at around  $2\theta = 20^\circ$  was observed indicating that the chitosan film was an amorphous state.

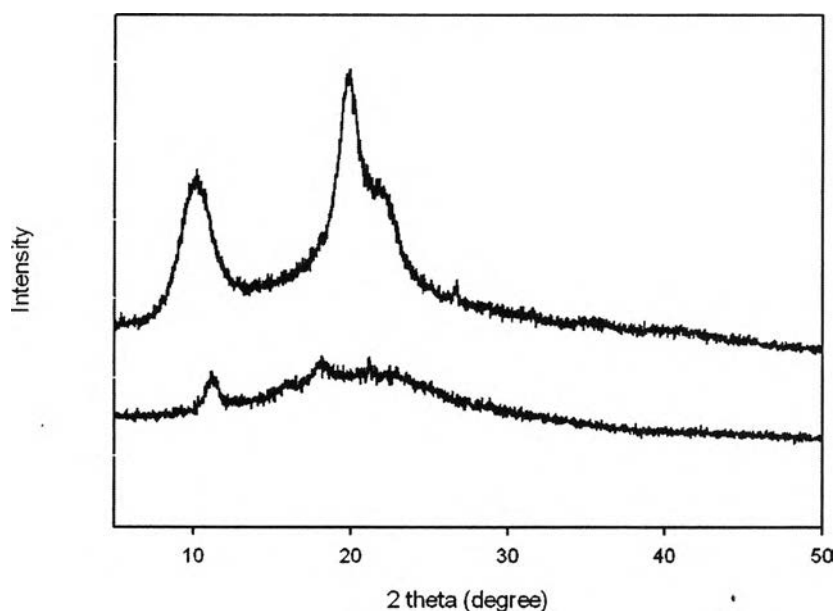


**Figure 4.2** The x-ray diffraction patterns of chitosan: (a) chitosan film (b) chitosan powder.

## 4.2 Preparation and Characterization of Polyaniline

### 4.2.1 UV-Visible Spectroscopy

The UV-Vis spectroscopy was used to investigate the electronic state of the NMP-soluble fraction of synthesized PANI in EB form. The result is shown in Figure 4.3. The EB form of PANI showed two absorption peaks at 320 and 620 nm which were due to the  $\pi$ - $\pi^*$  transition of the benzenoid ring and the exciton absorption of the quinoid ring, respectively (Cho, 2004). The integral areas under these two peaks indicated the concentration of the imine and the amine structure units as expected for the emeraldine oxidation state of PANI (Yang, 2003).

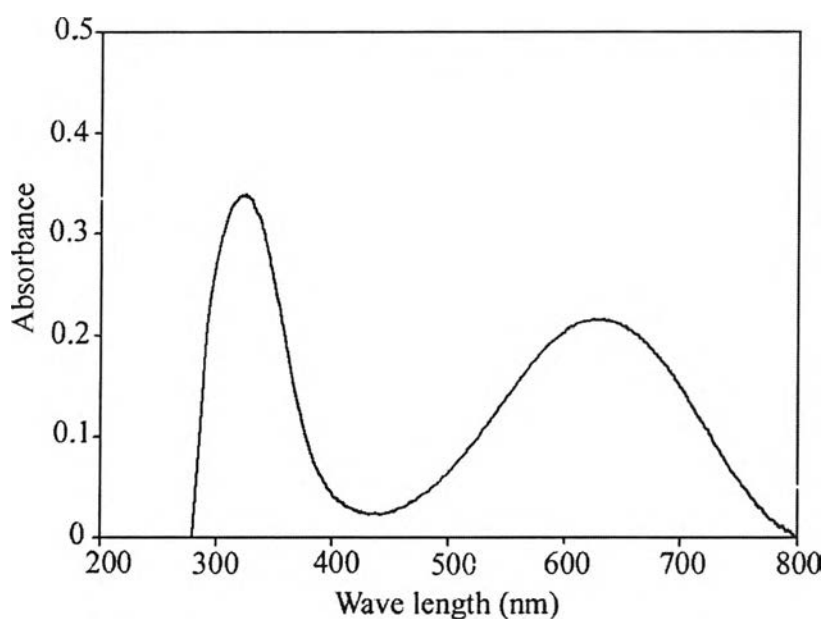


**Figure 4.3** UV-Vis spectrum of PANI in EB form.

### 4.2.2 X-Ray Diffractometry (XRD)

Figure 4.4 shows the x-ray diffraction patterns of undoped and doped PANI powder. For the undoped PANI, the broad peak observed between  $2\theta = 15$ - $25^\circ$  indicating an amorphous state of undoped PANI. After doping the undoped PANI with HCl, the diffraction patterns changed to the distinct sharp peaks appearing at  $2\theta = 9, 16, 21,$  and  $27^\circ$ . This implied that the structure of the doped PANI was in the crystalline state. The change in crystalline structure of PANI may be due to the

change in emeraldine base form (EB form) to the emeraldine salt form (ES form), which was highly symmetrical structure after doping process.

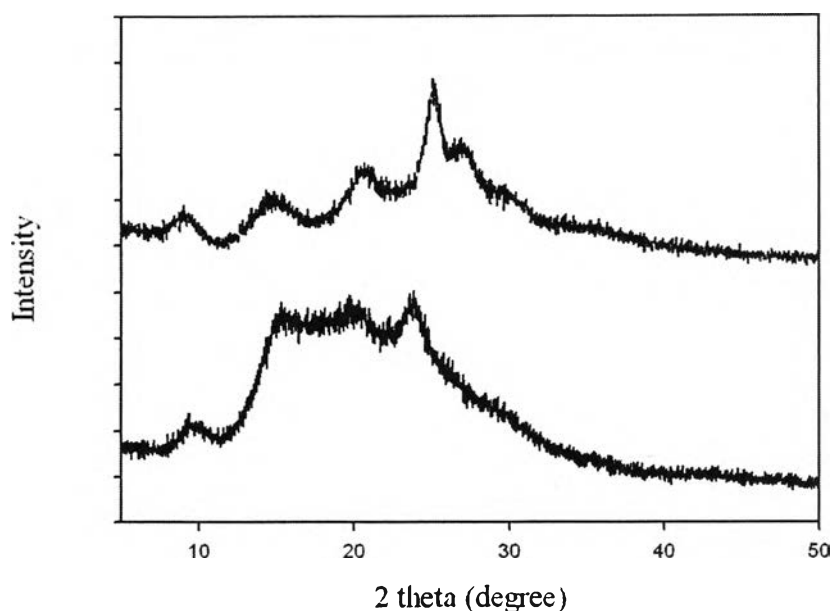


**Figure 4.4** The x-ray diffraction pattern of PANI powder: (a) undoped PANI powder and (b) doped PANI powder.

#### 4.2.3 Thermal Gravity Analysis (TGA)

The TGA thermogram used to compare the thermal behavior of undoped and doped PANI powder is shown in Figure 4.5. For the undoped PANI, two stage weight losses occurred at approximately 100°C and 500°C. While the doped PANI shows three stage weight loss. The first weight loss (ca. 100 °C) indicated the loss of water molecule in the PANI chain. The second weight loss occurring between 150°C and 250°C may be attributed to loss of acid dopant bound to the PANI chain (Gok, 2003). The final stage at about 500°C was due to the decomposition of PANI chain.

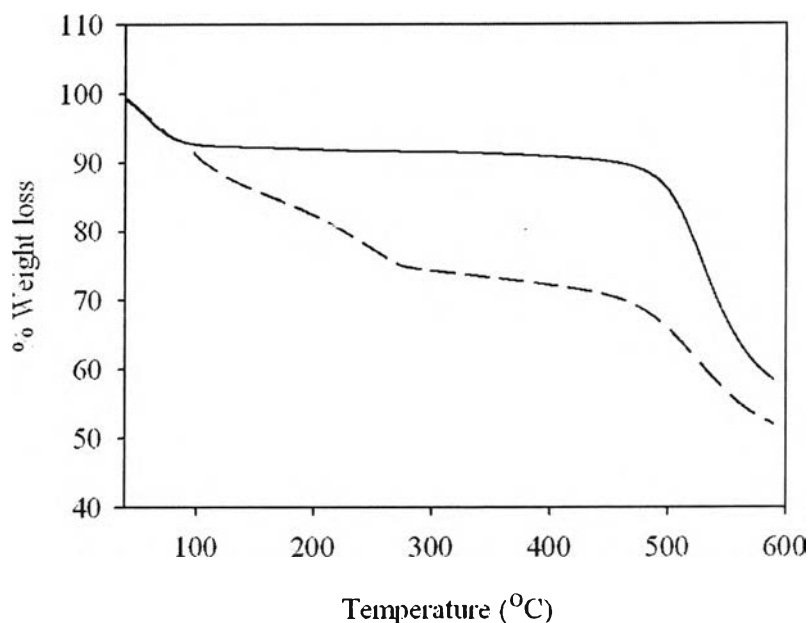


**Figure 4.5** The TGA thermogram of (a) doped PANI powder and (b) undoped PANI powder.

### 4.3 Preparation and Characterization of Polyaniline /Chitosan Blend Film

The blend of polyaniline and chitosan was prepared by blending the chitosan solution and polyaniline solution together. Due to the miscibility of each solvent (acetic acid and NMP), the homogenous blend was obtained. The smooth, flexible, and mechanically robust film was obtained by solution casting technique.

#### 4.3.1 FTIR Spectroscopy

FTIR spectra of PANI, chitosan, and PANI/chitosan blend films are shown in Figure 4.6. For pure chitosan, the absorption peak at  $3274\text{ cm}^{-1}$  was due to the overlapping of the OH and  $\text{NH}_2$  stretchings (Nunthanid, 2004). The peak appearing at  $1716\text{ cm}^{-1}$  was due to the C=O stretching in  $\text{NHCOCH}_3$ , arising from a small portion of pristine chitin which was not deacetylated during the N-acetylation (Sung, 2002). The absorption peaks at  $1548\text{ cm}^{-1}$  and  $1408\text{ cm}^{-1}$  could be assigned to the asymmetric and the symmetric stretchings of carboxylate anion, indicating that chitosan molecules in the film were in the form of chitosonium acetate (Puttipipatkachorn, 2004). For the FTIR spectrum of pure PANI in the emeraldine

base form, the absorption peaks observed at 1567, 1493, 1305, and 828  $\text{cm}^{-1}$  corresponding to the stretching of C=N bond of the quinoid structure, the stretching of the C-N bond of the benzenoid structure, the stretching of the C-H bond with aromatic conjugation, and the vibration of symmetrically substituted benzene, respectively (Zhang, 2002).

These characteristic absorption peaks could also be observed in the FTIR spectra of chitosan/PANI blends. As expected, in Figure 4.6, the characteristic absorption peaks of PANI became more dominant with increasing the PANI content.

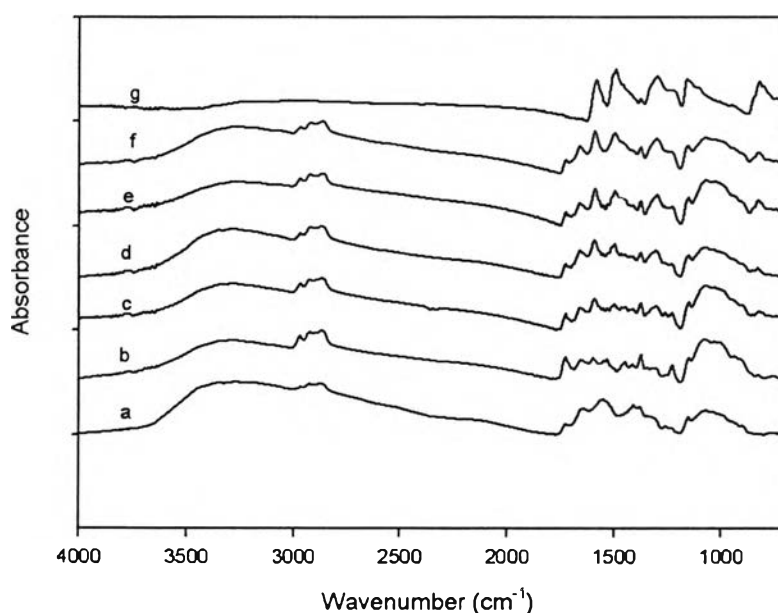


**Figure 4.6** FTIR spectra of PANI, chitosan, and PANI/chitosan blend films:

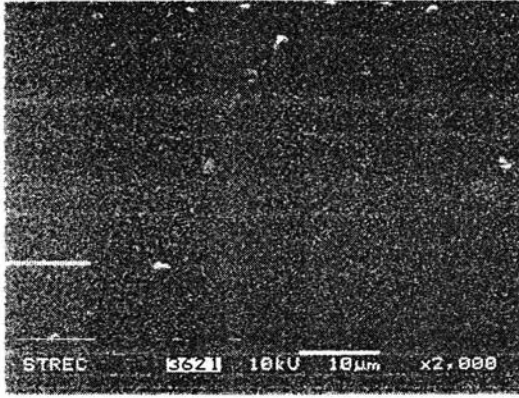
(a) chitosan, (b) 10 wt% PANI, (c) 20 wt% PANI, (d) 30 wt% PANI, (e) 40 wt% PANI, (f) 50 wt% PANI, and (g) PANI.

#### 4.3.2 Scanning Electron Microscope (SEM)

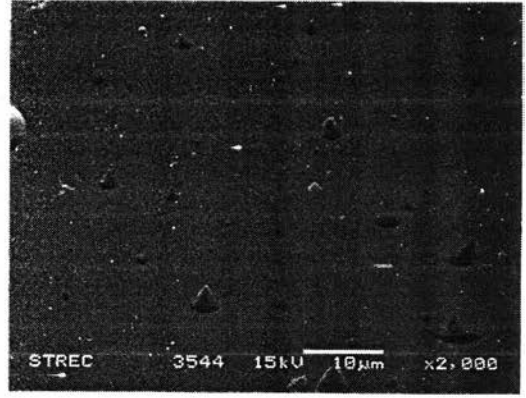
SEM images of the surface morphology of pure chitosan and the blend films at various PANI contents are shown in Figure 4.7. In order to investigate the distribution of PANI in the chitosan matrix, the NMP solvent was used as the extraction solvent to remove the PANI from the films. Pure chitosan film (Fig. 4.7a) showed a homogeneous featureless surface and there was no characteristic change in

morphology was observed after treatment with NMP (Fig. 4.7b). Chitosan did not dissolve in NMP, therefore, the original morphology was retained. On introducing the 10 wt% PANI into the chitosan matrix (Fig.4.7c), a smooth surface was still observed for the blend film. However, the small holes were seen after the extraction PANI particles with NMP (Fig. 4.7d). This could be attributed to the removal of PANI particles from the surface of the blend film. On increasing the PANI content from 20-50 wt%, the films showed a rough surface and the roughness increased after treatment with NMP (Fig. 4.7e-4.7l).

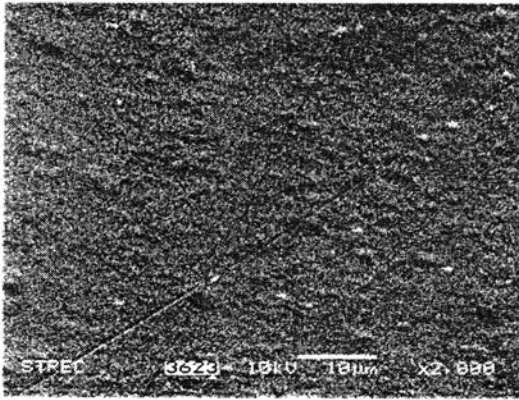




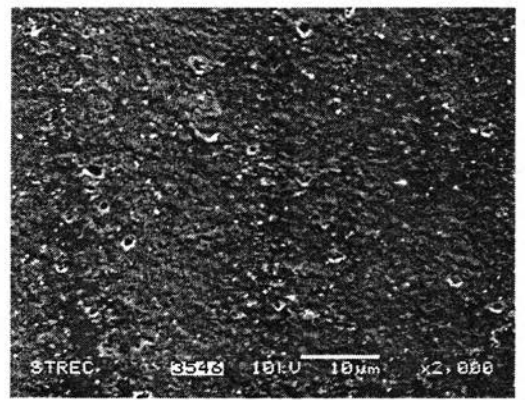
a



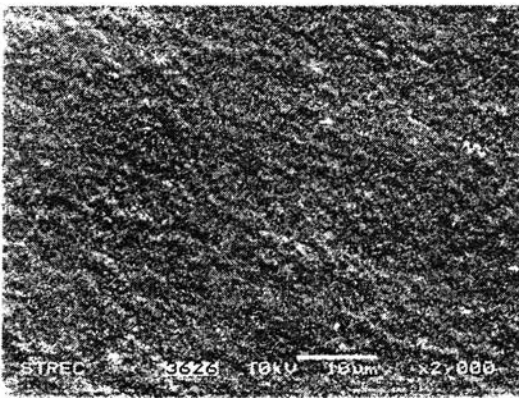
b



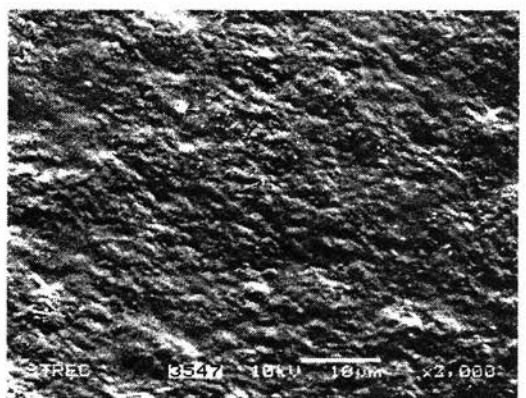
c



d



e



f

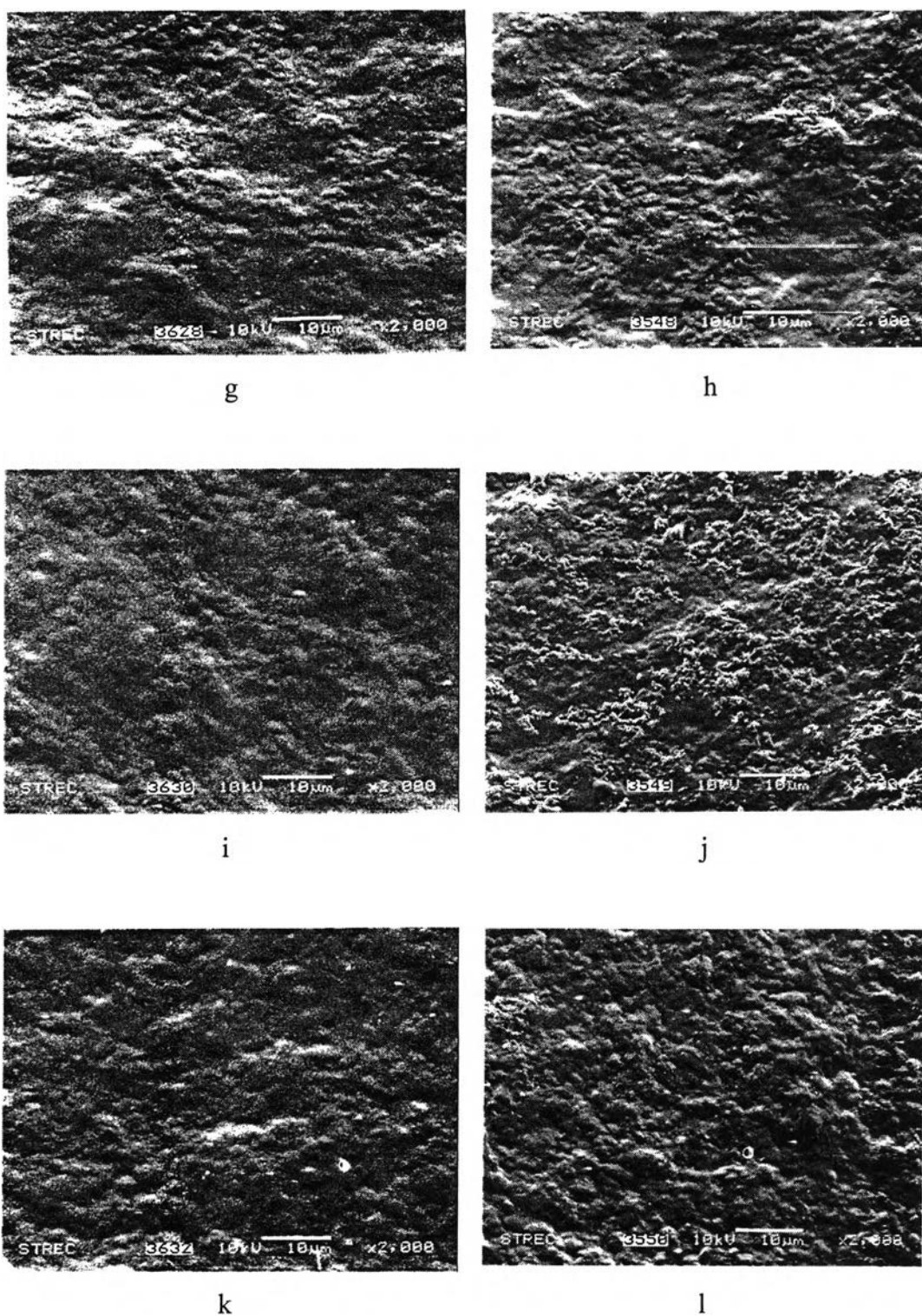


**Figure 4.7** SEM micrographs of the surface morphology of the PANI/chitosan blend films before and after treated with NMP solvent: (a) untreated chitosan, (b) treated chitosan, (c) untreated 10 wt% PANI, (d) treated 10 wt% PANI, (e) untreated 20 wt% PANI, (f) treated 20 wt% PANI, (g) untreated 30 wt% PANI, (h) treated 30

wt% PANI, (i) untreated 40 wt% PANI, (j) treated 40 wt% PANI, (k) untreated 50 wt% PANI, (l) treated 50 wt% PANI.

Figure 4.8 shows SEM images of the cross-sectional fracture surface of pure chitosan and the PANI/chitosan blend films with various blend compositions. The cross-sectional morphology is the one of the technique used to investigate the miscibility of two component in the blend film. For the pure chitosan (Fig. 4.8a), the homogenous morphology was observed. However, when adding the PANI into the chitosan, they clearly showed that PANI particles were dispersed uniformly throughout the chitosan matrix when the content of PANI was lower than 50 wt% (Figs 4.8b-4.8e). Apparent voids or cracks were found in the blend with 50 wt% PANI (Fig 4.8f). This might be due to the immiscible blend of PANI and chitosan occurred when increasing the PANI content up to 50 wt%. Our results could be compared with previous studied of PANI- $\beta$ -NSA/PVA blend films (Zhang, 2002). These authors reported that PANI- $\beta$ -NSA particles were dispersed uniformly in the PVA matrix when the content of PANI- $\beta$ -NSA was lower than 12.6 wt% and distinct aggregates of PANI- $\beta$ -NSA were observed when the content of PANI- $\beta$ -NSA was increased to 49 wt%.

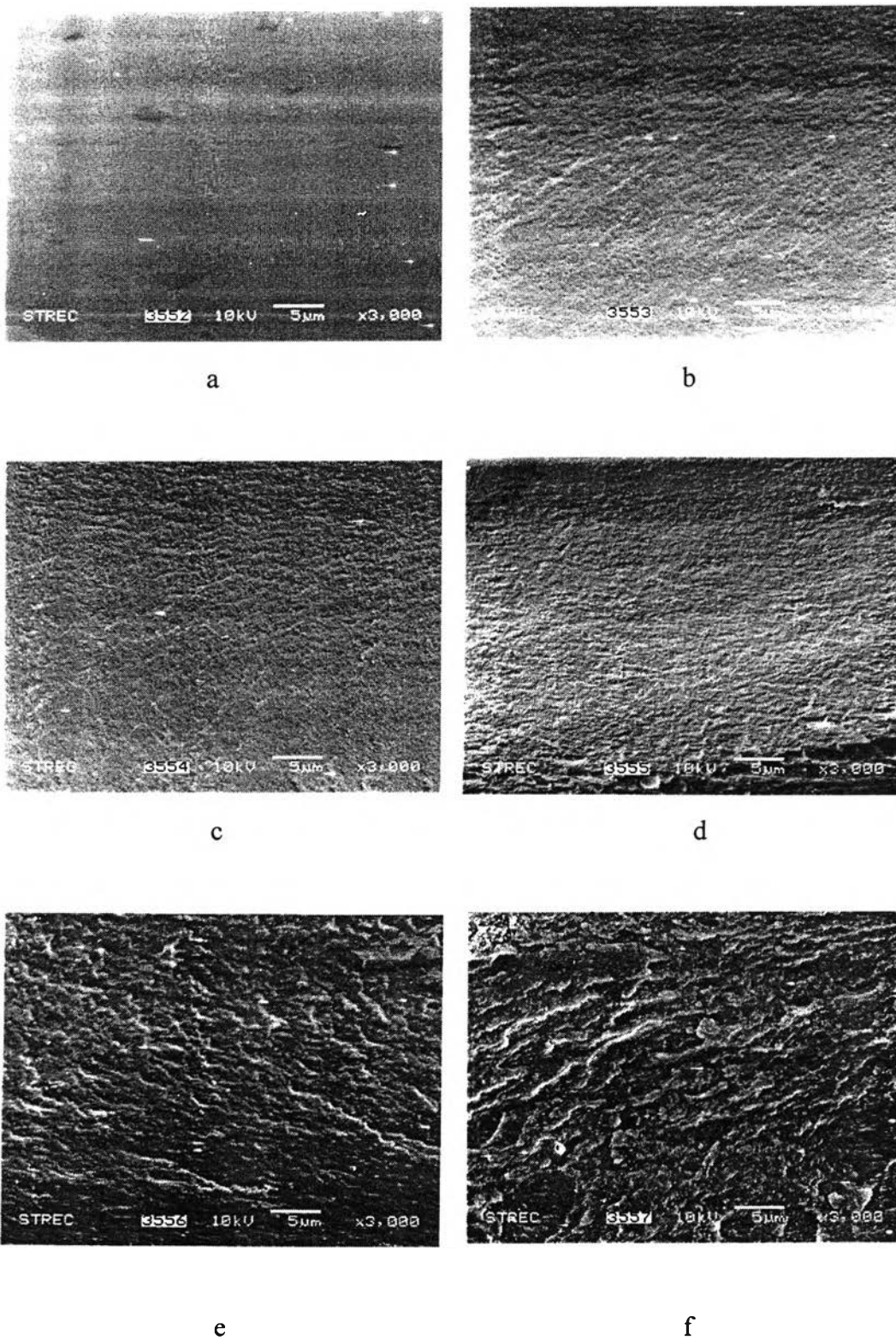


**Figure 4.8** The cross-sectional SEM micrographs of pure chitosan film and the blend films: (a) chitosan film, (b) 10 wt% PANI, (c) 20wt% PANI, (d) 30 wt% PANI, (e) 40 wt% PANI, and (f) 50 wt% PANI.

### 4.3.3 X-Ray Diffractometry (XRD)

Wide-angle x-ray diffraction (WAXD) patterns were used to study the crystalline structure of pure chitosan, polyaniline and their blend films in the undoped and doped form as shown in Figure 4.9 and Figure 4.10, respectively. As mention in previous part, the chitosan film showed the crystalline peak at  $2\theta = 11^\circ$  and a broad peak centered at  $2\theta = 20^\circ$ . Where as, the diffraction pattern of polyaniline in EB form showed a small peak near  $10^\circ$  and a group of broad peaks in the range  $2\theta = 15-25^\circ$ . These results suggested that the structures of chitosan and polyaniline in EB form were mostly amorphous. For the blend films, the diffraction peak at  $2\theta = 11^\circ$  vanished at all compositions while the diffraction peak centered at  $2\theta = 20^\circ$  become sharper with increasing PANI content. This implied that the addition of PANI into the chitosan matrix resulted in a specific interaction between PANI and chitosan chain which lowered the degree of crystallinity of the chitosan matrix.

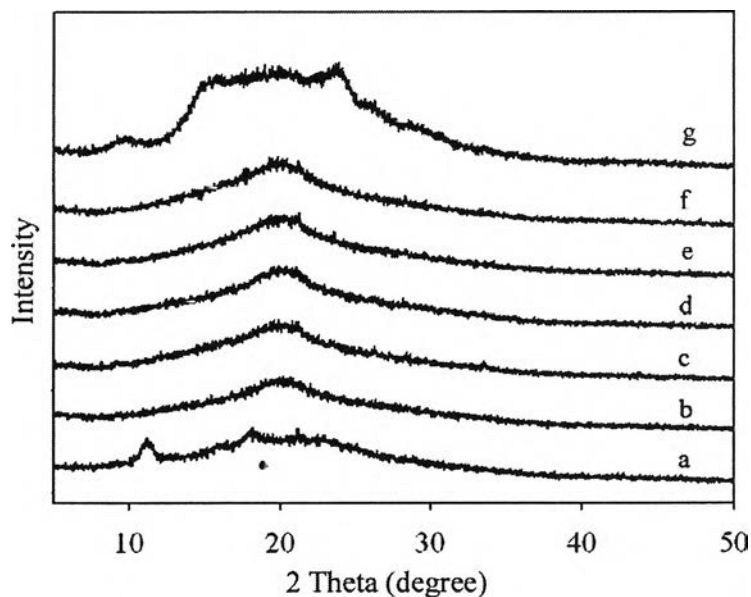


**Figure 4.9** The x-ray diffraction pattern of undoped chitosan film, polyaniline powder, and the blend films: (a) chitosan film, (b) 10 wt% PANI, (c) 20 wt% PANI, (d) 30 wt% PANI, (e) 40 wt% PANI, (f) 50 wt% PANI, and (g) PANI.

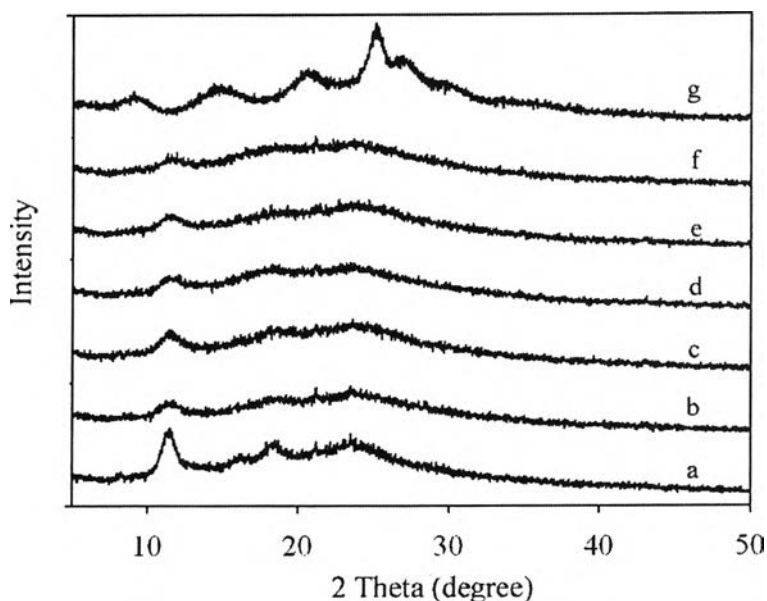


**Figure 4.10** The x-ray diffraction pattern of doped chitosan film, polyaniline powder, and the blend films with 1 M HCl for 10 hrs: (a) chitosan film, (b) 10 wt% PANI, (c) 20 wt% PANI, (d) 30 wt% PANI, (e) 40 wt% PANI, (f) 50 wt% PANI, and (g) PANI.

The XRD diffraction patterns of doped chitosan and blend films with HCl solutions were used to investigate the change in crystalline structure of chitosan and their blend films as compared to undoped films. For the chitosan film, the intensity of the crystalline peak at  $2\theta = 11^\circ$  increased after doping with HCl solution. Similar to chitosan, the diffraction patterns of the blend films at all compositions had a distinct crystalline peak at  $2\theta = 11^\circ$  after doping with HCl solution. This may be due to the ions exchange between acetate ions in the chitosan structure and the chloride ion of the acid dopant. The smaller size of chloride ions induced a better packing between the chitosan and the PANI structures.

#### 4.3.4 Differential Scanning Calorimetry (DSC)

DSC thermograms of PANI, chitosan, and the blend films are shown in Figure 4.11. DSC thermogram of pure PANI showed an endothermic peak at around  $120^\circ\text{C}$  owing to the evaporation of water molecules. Meanwhile, Broad

exothermic peaks observed between 200 and 400°C, may be a result of the interchain interaction such as H-bonding between PANI chains. Another exothermic peak appeared in pure PANI at 500°C corresponding to the degradation of the PANI backbone (Gok, 2003). In contrast, pure chitosan exhibited an endothermic peak at approximately 120°C followed by an exothermic peak at 290°C. These peaks indicated loss of water and the degradation of chitosan, respectively (Kittur, 2001).

For the blend films, the degradation process took place at temperatures higher than pure chitosan, indicating that the thermal stability of the composite films was higher than that of chitosan alone. Moreover, an exothermic peak at around 200°C could be observed in the blend films containing 30-50 wt% of PANI. This may support the claim that the partially interchain interaction of PANI chains occurred with increasing PANI content.

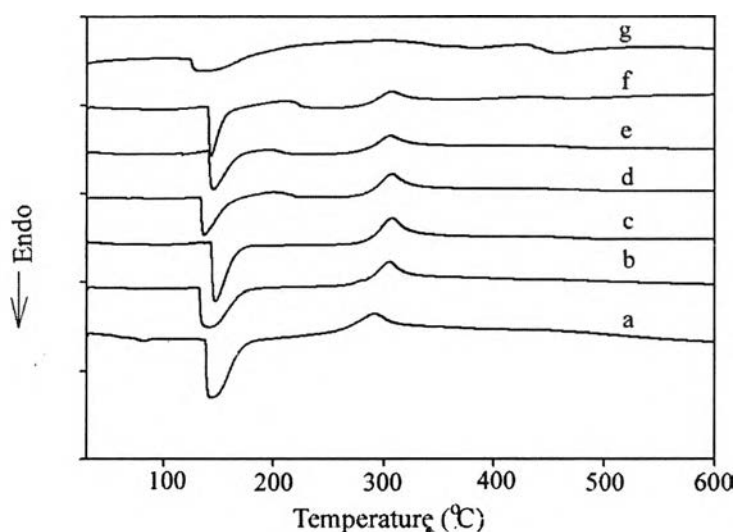


**Figure 4.11** DSC thermograms of chitosan, polyaniline, and the blend films:

(a) chitosan, (b) 10 wt% PANI, (c) 20 wt% PANI, (d) 30 wt% PANI, (e) 40 wt% PANI, (f) 50 wt % PANI, and (g) PANI.

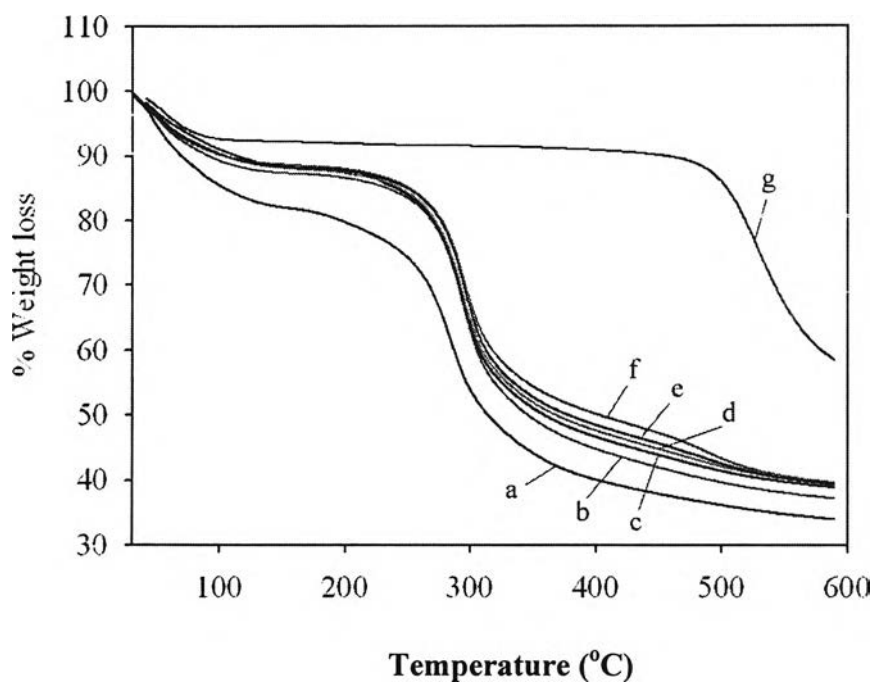




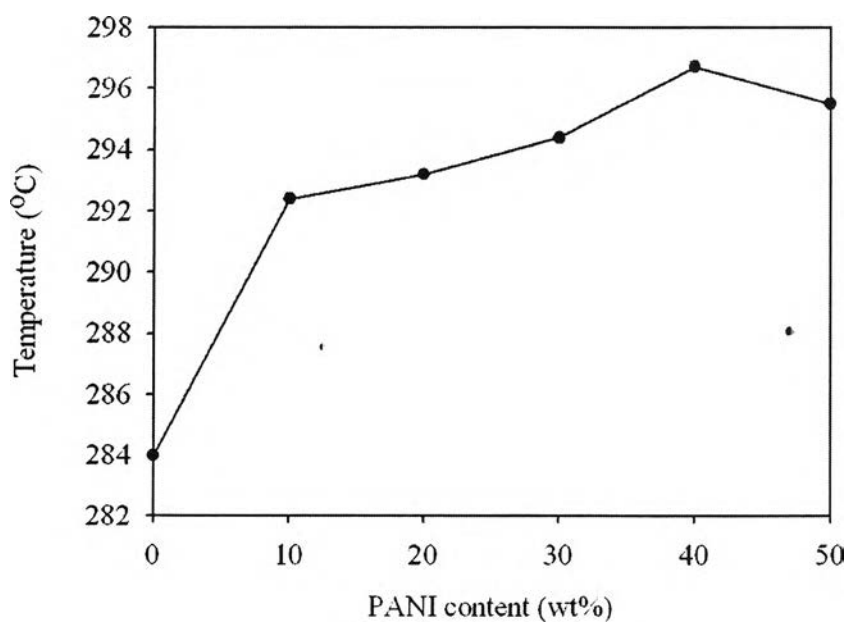
#### 4.3.5 Thermal Gravity Analysis (TGA)

Figure 4.12 shows the TGA thermogram of the PANI, chitosan, and their blend films. For pure PANI, two discrete weight losses occurred at approximately 100°C and 500°C corresponding to loss of water and the degradation of PANI chains, respectively. In comparison, chitosan showed two discrete weight losses at approximately 100°C and 284°C reflecting loss of water and the degradation of chitosan chains, respectively. Similar to chitosan, the blend films containing 10-40 wt% PANI content exhibited two weight loss steps due to the evaporation of water and the degradation of the blend films. The degradation temperature ( $T_d$ ) of the composite films increased with increasing PANI content, as shown in Figure 4.13. This result correlated with the DSC thermogram and suggested that there was an intermolecular interaction, such as hydrogen bonding, between PANI and chitosan chains. In contrast, the blend film containing 50 wt% PANI content exhibited two distinct degradation temperatures at approximately 295 °C and 500 °C. This implied that partially phase separation occurred. The first temperature occurred at  $T_d$  of chitosan and the second temperature occurred at  $T_d$  of PANI.





**Figure 4.12** The TGA thermogram of undoped chitosan, polyaniline, and the blend film: (a) chitosan, (b) 10 wt% PANI, (c) 20 wt% PANI, (d) 30 wt% PANI, (e) 40 wt% PANI, (f) 50 wt % PANI, and (g) PANI.



**Figure 4.13** The degradation temperature ( $T_d$ ) of PANI/chitosan blend films.

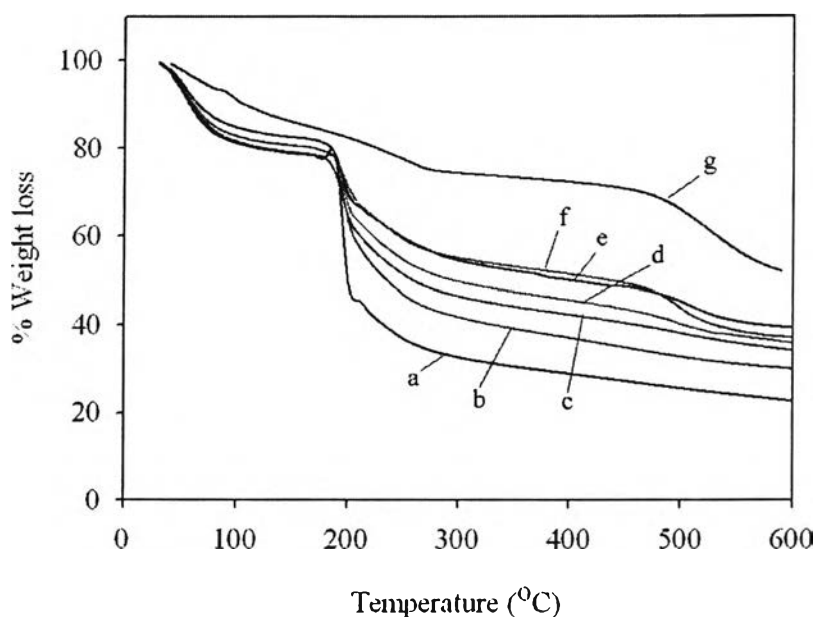


**Figure 4.14** The TGA thermogram of doped chitosan, polyaniline, and the blend film with 1 M HCl for 10 h: (a) chitosan, (b) 10 wt% PANI, (c) 20 wt% PANI, (d) 30 wt% PANI, (e) 40 wt% PANI, (f) 50 wt % PANI, and (g) PANI.

The TGA thermograms of the PANI, chitosan, and blend films after doping with HCl solution are shown in Figure 4.14. We observed that the chitosan and blend films exhibited a lower  $T_d$  (ca. 200°C) as compared to those of the undoped films (ca. 295°C). This may be due to the acid hydrolysis process causing chitosan chain scission during the doping process.

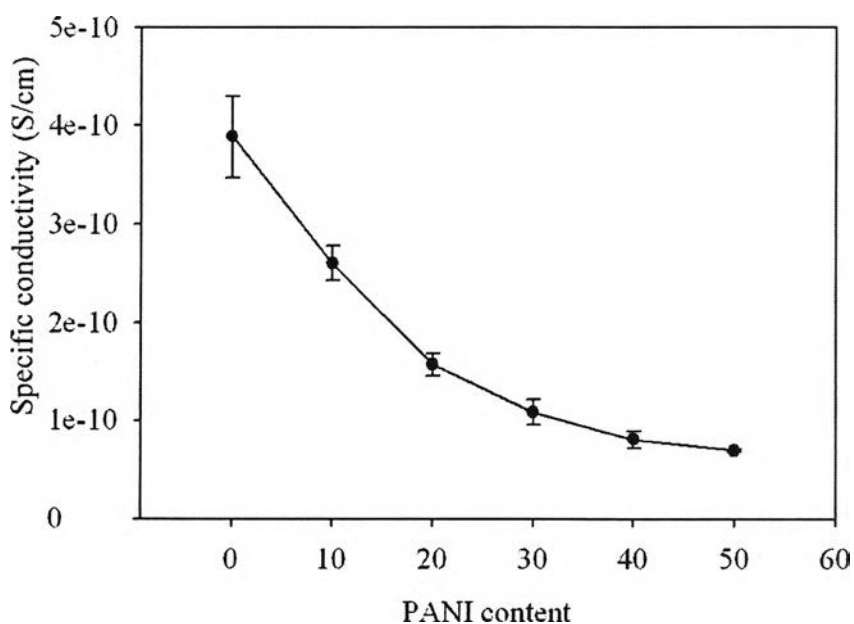
#### 4.3.6 Electrical Property

Room temperature DC electrical conductivity values of PANI/chitosan blend films were measured before and after doping with various HCl concentrations, doping times, and different types of acid dopant. The doping stage was noticeable as a distinct color change of the films from blue to green.

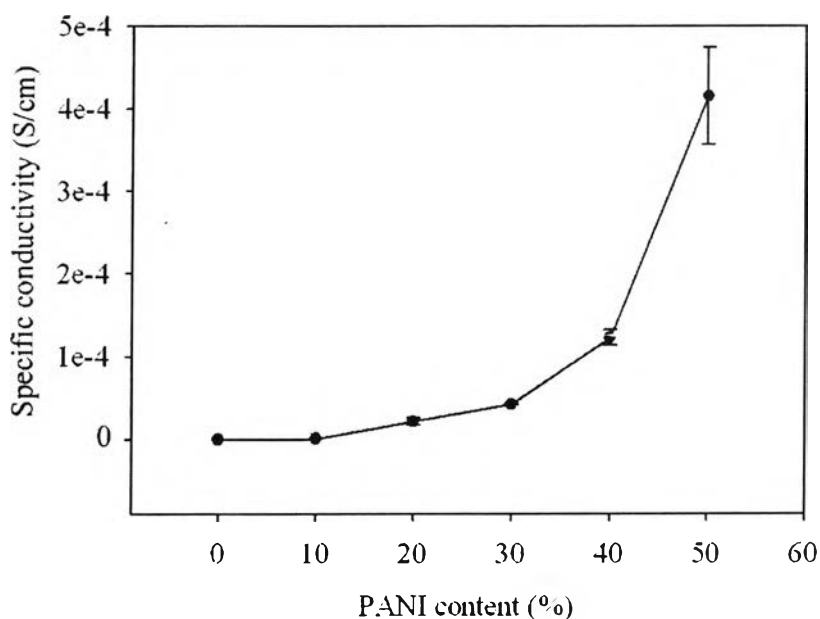
##### 4.3.6.1 *Effect of Blend Composition*

Figure 4.15 shows the electrical conductivity of undoped PANI/chitosan blend films as a function of PANI content. The data are also listed in Table 4.3, and indicated that the electrical conductivity of the blend films decreased with increasing PANI content. Pure chitosan had appreciable

conductivity, ca.  $3.38 \times 10^{-10}$  S/cm, due to the polarity of the protonated amino group of the chitosonium acetate. On addition of the PANI EB, the insulating form of PANI, the ionic mobility of chitosonium acetate was disrupted, resulting in a decrease of electrical conductivity. On the other hand, after the blend films were doped with 0.5 M HCl for 2 h, the electrical conductivity of the blend films increased significantly with increasing PANI content as shown in Figure 4.16 and also listed in Table 4.3. This was a direct result of the conversion of the emeraldine base form to the emeraldine salt form, which is a highly  $\pi$ -conjugated system. In addition, we found that the blend films with PANI content higher than 50 wt% could not be fabricated due to excessive film brittleness.



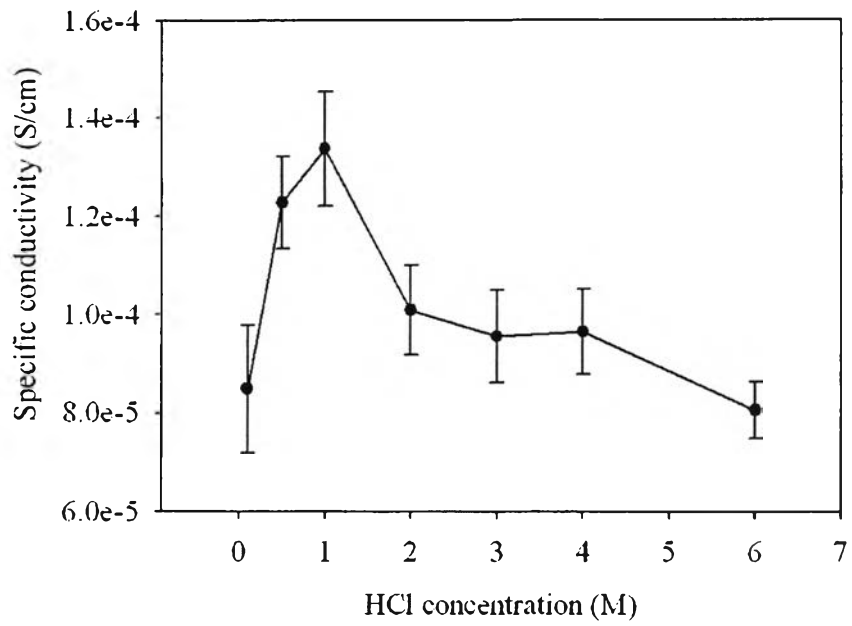
**Figure 4.15** Specific conductivity of undoped PANI/chitosan composite films as a function of PANI content.



**Figure 4.16** Specific conductivity of doped PANI/chitosan composite films as a function of PANI content.

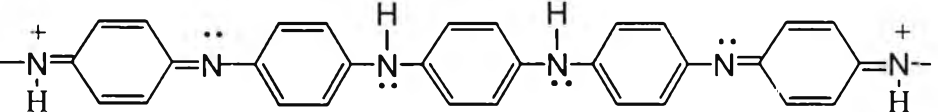
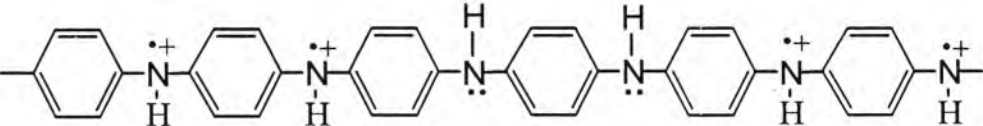
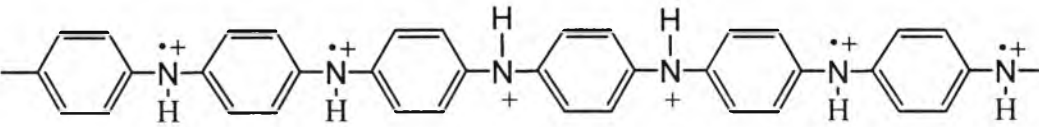
#### 4.3.6.2 Effect of Hydrochloric Concentration

The effect of HCl concentration, used as a dopant, on the electrical conductivity of the blend films at a 40 wt% PANI content was investigated and the results are shown in Figure 4.17 and also listed in Table 4.4. The electrical conductivity of the films increased when HCl concentration increased from 0.1 M to 1 M. The enhancement of the electrical conductivity with increasing HCl concentration was due to the increasing degree of protonation of the imine group of PANI. At higher HCl concentration (2 M-6 M HCl), a decrease in electrical conductivity occurred. This result was probably due to the over protonation of PANI chains causing a decrease in the delocalization length of PANI. The proposed model for explanation the electrical conductivity of the doped PANI/chitosan blend film as a function of acid concentrations was shown in Table 4.2.



**Figure 4.17** Specific conductivity of doped PANI/chitosan composite films as a function of HCl concentration.

**Table 4.2** The proposed structures of doped<sup>a</sup> PANI/chitosan blend film as a function of acid concentrations

HCl concentration (M)	Explanations	The propose structures
0.1	<ul style="list-style-type: none"> <li>- Some protonation at quinoid structures</li> <li>- Lower the electrical conductivity</li> </ul>	
1	<ul style="list-style-type: none"> <li>- Equilibrium protonation at quinoid structure</li> <li>- The delocalization of electrons in the interchain direction</li> <li>- Maximum the electrical conductivity</li> </ul>	
>1	<ul style="list-style-type: none"> <li>- Shorten delocalization lengths</li> <li>- Electron delocalization only in the shorten limited length in intrachain direction</li> <li>- Lower the electrical conductivity</li> </ul>	

<sup>a</sup> The blend films with 40 wt % PANI content and 2 h of doping time were used.

#### 4.3.6.3 Effect of Doping Time

Figure 4.18 reveals that the electrical conductivity of the blend films varied with the doping time. The results are also listed in Table 4.5. The electrical conductivity of the blend films increased with increase of doping time from 0.5 h to 10 h. Doping times longer than 10 h led to a decrease in electrical conductivity. This was a result of the over protonation of PANI occurring at prolonged doping times.

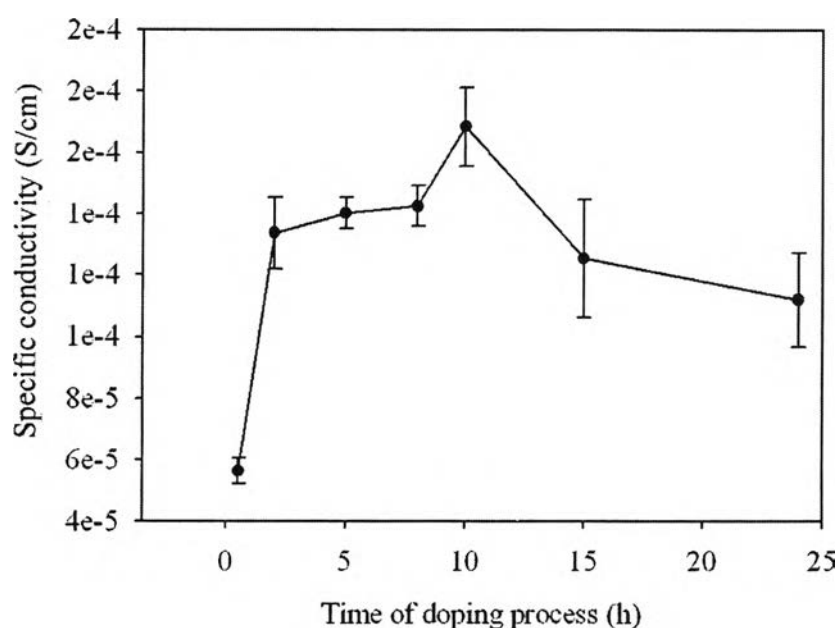


**Figure 4.18** Specific conductivity of doped PANI/chitosan composite films as a function of doping time.

#### 4.3.6.4 Effect of Type of Acid Dopant

Table 4.6 shows the electrical conductivity of the blend films doped with different types of acid dopant. The nature of acid dopant, which involved a change in the strength and the size of the acid dopant molecule, evidently affected the electrical conductivity of the blend films, which increased with increasing acid strength. This increase in electrical conductivity was due to the enhancement of degree of protonation of the imine group of PANI. The size of acid dopant also influenced the electrical conductivity of blend films. The electrical conductivity of the blend films decreased as the dopant anion size increased. Larger anions could more easily disrupt the orientation of PANI chains causing a lower degree of PANI

chain packing. Hence, the electrical conductivity of the blend films decreased with increasing anion size.

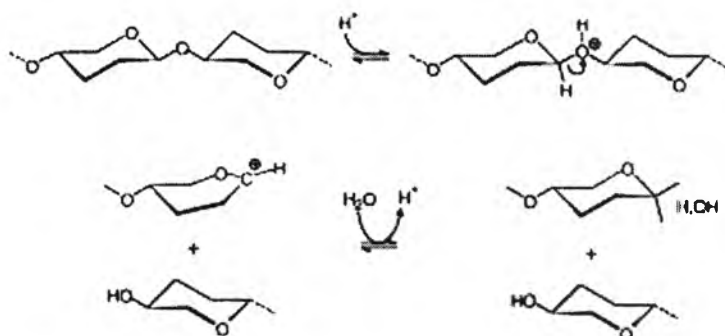
#### 4.3.7 Mechanical Properties

The mechanical properties of the blend films at various blend compositions are shown in Table 4.3. Chitosan itself formed films with high values of the tensile strength and the modulus; they were 68 and 2912 MPa, respectively. On addition of 10 wt% of PANI, the tensile strength and the modulus of the blend films decreased because the small amount of PANI disrupted the chitosan network. However, both tensile strength and the modulus increased to some extent with increasing of PANI content from 20 to 40 wt%. This may be attributed to a more uniform combination of PANI and chitosan. Upon introducing more PANI up to 50 wt% in the blends, the inhomogeneity of the blend solution occurred during blending the two polymers resulting in the decrease of tensile strength and modulus. Furthermore, the elongation at break tended to decrease with increasing PANI content indicating that the blend films became more brittle with increasing the PANI content. Our result agreed with those of previous works (Mirmohseni, 2003), (Gamgopadhyay, 2002) which reported that a small amount of PANI (9 wt%) in the PVA matrix could cause a decrease in tensile strength. On increasing the PANI content to 17 wt% the tensile strength increased due to the more uniform combination of PANI and PVA matrix and the tensile strength dropped again after adding more PANI content. These results implied that the processability of polyaniline could be improved by blending PANI with some soluble polymers as a matrix (Zhang, 2002).

After doping the blend films with HCl solution, the tensile strength and the modulus decreased at all PANI compositions. Increase in HCl concentration and doping time caused a decrease in the tensile strength and the modulus as shown in Table 4.4 and Table 4.5, respectively. This result may be due to the degradation of the chitosan network which acted as the matrix of the blend films (Varum, 2001 and Jia, 2002) and also due to the well known fact that PANI becomes more crystalline at a higher doping levels. In addition to the effects of HCl concentration and doping time, the type of acid dopant could also affect the mechanical properties as shown in Table 4.6. The mechanical properties dramatically decreased with higher strength of



acid dopant because the higher strength of acid caused a higher degree of chitosan chain scission in the blend films. The purpose mechanism of chitosan degradation is shown in Scheme 4.1.



**Scheme 4.1** The purpose reaction mechanism for acid hydrolysis of glycosidic linkage in chitosan chain.

**Table 4.3** Specific conductivity and mechanical properties of the undoped and doped<sup>a</sup> PANI/chitosan blend films as a function of PANI content

PANI Content (%)	Specific conductivity (S/cm)		Young's modulus (MPa)		Tensile strength (MPa)		Elongation at break (%)	
	Before doping	After doping	Before doping	After doping	Before doping	After doping	Before doping	After doping
0	3.38E-10	7.56E-8	2912.85±570.03	2063.30±357.33	68.31±4.78	41.02±4.30	17.02±1.56	5.96±0.92
10	2.60E-10	7.69E-7	2828.82±296.84	1679.95±337.85	58.35±3.97	32.31±3.66	7.58±1.09	7.23±1.71
20	2.57E-10	2.15E-5	2970.62±360.25	2173.90±352.00	75.49±3.27	46.69±4.34	7.54±0.84	6.21±1.20
30	1.08E-10	4.27E-5	3212.83±242.27	2179.61±191.49	81.76±2.80	49.13±4.51	7.29±0.85	5.82±1.08
40	8.09E-11	1.23E-4	3138.73±504.88	2430.74±434.00	83.99±2.27	52.15±5.74	7.00±0.92	8.13±0.79
50	6.97E-11	4.16E-4	2689.43±386.89	2279.47±217.85	75.08±4.69	43.16±3.42	6.74±1.02	4.75±1.09

<sup>a</sup> The blend films were doped with 0.5 M HCl for 2 h.

**Table 4.4** Specific conductivity and mechanical properties of the undoped and doped<sup>a</sup> PANI/chitosan blend films as a function of HCl concentrations

HCl concentration	Specific conductivity (S/cm)		Young's modulus (MPa)		Tensile strength (MPa)		Elongation at break (%)	
	Before doping	After doping	Before doping	After doping	Before doping	After doping	Before doping	After doping
0.1	8.09E-11	8.50E-5	3138.73±504.88	2434.93±316.00	83.99±2.27	53.23±2.97	7.00±0.92	11.35±1.53
0.5	8.09E-11	1.23E-4	3138.73±504.88	2430.74±434.00	83.99±2.27	52.15±5.74	7.00±0.92	8.13±0.79
1.0	8.09E-11	1.34E-4	3138.73±504.88	2149.15±310.36	83.99±2.27	51.46±3.99	7.00±0.92	7.58±1.05
2.0	8.09E-11	1.01E-4	3138.73±504.88	2160.82±164.18	83.99±2.27	49.43±3.75	7.00±0.92	6.82±1.06
3.0	8.09E-11	9.58E-5	3138.73±504.88	2199.77±209.19	83.99±2.27	49.22±3.76	7.00±0.92	6.08±0.89
4.0	8.09E-11	9.67E-5	3138.73±504.88	2022.83±229.53	83.99±2.27	48.46±5.39	7.00±0.92	6.29±0.90
6.0	8.09E-11	8.07E-5	3138.73±504.88	2101.30±237.70	83.99±2.27	46.33±4.48	7.00±0.92	4.10±0.89

<sup>a</sup> The blend films with 40 wt % PANI content and 2 h of doping time were used.

**Table 4.5** Specific conductivity and mechanical properties of the undoped and doped<sup>a</sup> PANI/chitosan blend films as a function of doping time

Doping time	Specific conductivity (S/cm)		Young's modulus (MPa)		Tensile strength (MPa)		Elongation at break (%)	
	Before doping	After doping	Before doping	After doping	Before doping	After doping	Before doping	After doping
0.5	8.09E-11	5.65E-5	3138.73±504.88	2236.76±262.37	83.99±2.27	53.04±4.15	7.00±0.92	5.92±0.54
2.0	8.09E-11	1.34E-4	3138.73±504.88	2149.15±310.35	83.99±2.27	51.46±3.99	7.00±0.92	7.58±1.05
5.0	8.09E-11	1.40E-4	3138.73±504.88	2055.75±296.14	83.99±2.27	50.55±4.30	7.00±0.92	6.69±0.86
8.0	8.09E-11	1.43E-4	3138.73±504.88	2067.21±250.57	83.99±2.27	49.16±4.14	7.00±0.92	6.26±0.47
10.0	8.09E-11	1.69E-4	3138.73±504.88	1948.19±259.62	83.99±2.27	48.52±3.98	7.00±0.92	6.54±0.92
15.0	8.09E-11	1.25E-4	3138.73±504.88	1881.47±263.92	83.99±2.27	42.35±3.85	7.00±0.92	7.00±1.18
24.0	8.09E-11	1.12E-4	3138.73±504.88	1708.73±346.14	83.99±2.27	41.36±3.57	7.00±0.92	8.31±1.67

<sup>a</sup> The blend films with 40 wt % PANI content and doped with 1 M HCl were used.

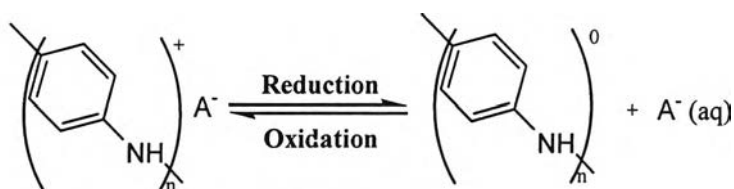
**Table 4.6** Specific conductivity and mechanical properties of PANI/chitosan blend films as a function of type of acid dopant

Type of acid dopant	pK <sub>a</sub>	Specific conductivity (S/cm)		Young's modulus (MPa)		Tensile strength (MPa)		Elongation at break (%)	
		Before doping	After doping	Before doping	After doping	Before doping	After doping	Before doping	After doping
Formic acid	3.75	8.09E-11	6.22E-8	3138.73±504.9	2234.86±355.28	83.99±2.27	60.69±5.65	7.00±0.92	13.71±1.67
Acetic acid	4.7	8.09E-11	2.01E-8	3138.73±504.9	2928.49±403.61	83.99±2.27	61.82±5.09	7.00±0.92	10.74±1.47
Ascorbic acid	4.2	8.09E-11	2.36E-10	3138.73±504.9	2762.30±471.33	83.99±2.27	75.19±4.11	7.00±0.92	6.11±1.02
Sulfuric acid	-3	8.09E-11	1.94E-4	3138.73±504.9	2573.97±250.80	83.99±2.27	48.25±4.09	7.00±0.92	7.15±1.28
Nitric acid	-1	8.09E-11	1.02E-4	3138.73±504.9	2474.65±260.07	83.99±2.27	51.68±3.67	7.00±0.92	8.06±0.91
Prechloric acid	-7	8.09E-11	4.07E-5	3138.73±504.9	2266.98±395.67	83.99±2.27	40.75±5.63	7.00±0.92	7.20±1.75
Hydrochloric acid	-6.1	8.09E-11	1.34E-4	3138.73±504.9	1927.93±267.22	83.99±2.27	47.43±5.31	7.00±0.92	6.54±0.92
p-toluene-sulfonic acid	-2.8	8.09E-11	1.42E-5	3138.73±504.9	2497.00±414.44	83.99±2.27	47.29±4.15	7.00±0.92	7.05±1.04

<sup>a</sup> The blend films with 40 wt % PANI content doped with 1 M of acid concentration for 10 hours were used except the concentration of ascorbic acid was 0.1 M.

#### 4.4 Drug Release Study

The effect of electrical field on drug release behavior of polyaniline/chitosan blend film was investigated and the result is shown in Figure 4.19. In this study, the PANI/chitosan blend film with 40 wt% PANI content was used as the drug carrier to study the release behavior of drug model. The experiment was done via modified Franz diffusion cell, a device for study transdermal permeation of drug. The 10 wt% of salicylic acid, used as the drug model, was loaded into the blend film by mixing the drug model into the mixture solution of chitosan, polyaniline in EB form, and glutaraldehyde. Due to the acidity of salicylic acid, the protonation at imine group of PANI in EB form was occurred during the blending process causing the change of PANI in EB form (oxidation no. = 0) to ES form (oxidation no. = +1). The salicylate anions were incorporated into the structure of PANI in ES form by ionic interaction as shown in Scheme 4.2. This caused the lowering amount of drug release. In contrast, when applying 1 V of electrical potential, the ES form of polyaniline (oxidation no. = +1) gained electrons and converted to the EB form (oxidation no. = 0) that minimized the interaction between polyaniline structure and the drug ions resulting in the increase of drug release.



**Scheme 4.2** The interconversion between doped and undoped state of polyaniline.

Massoumi et al. 2000 reported that one of the unique aspects of conductive polymer is their ability to be redox switch between doped (conducting) and undoped (insulating) state and the interconversion between these two states can be induced by electrochemical process (Kontturi et al., 1998). Therefore, this can provide the ability to use in the application of electrically stimulated controlled release. For the cationic drug ions, the drug ions are incorporated into cation dominant conductive

polymers during reduction and anodically released. In contrast, the anionic drug can be cathodically released.

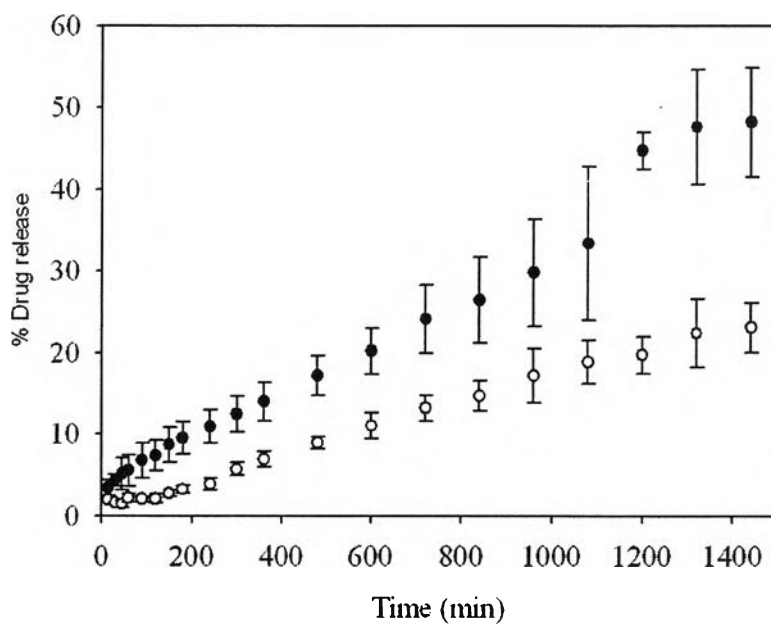


**Figure 4.19** The drug release study of PANI/chitosan blend film with 40 wt% PANI content as a function of time: (●) with 1 volt of electrical potential, (○) without an electrical potential.